DISK ACCRETION ONTO HIGH-MASS PLANETS

S. H. LUBOW,[1] M. SEIBERT,[1,2] AND P. ARTYMOWICZ[3]

ABSTRACT

We analyze the nonlinear, two-dimensional response of a gaseous, viscous protoplanetary disk to the presence of a planet of one Jupiter mass (1 M_J) and greater that orbits a 1 $M_\odot$ star by using the ZEUS hydrodynamics code with high resolution near the planet's Roche lobe. The planet is assumed to be in a circular orbit around the central star and is not allowed to migrate. A gap is formed about the orbit of the planet, but there is a nonaxisymmetric flow through the gap and onto the planet. The gap partitions the disk into an inner (outer) disk that extends inside (outside) the planet's orbit. For a 1 M_J planet and typical disk parameters, the accretion through the gap onto the planet is highly efficient. That is, the rate is comparable to the accretion rate toward the central star that would occur in the absence of the planet (at the location of the planet). For typical disk parameters, the mass-doubling timescale is less than 10^5 yr, considerably shorter than the disk lifetime. Following shocks near the $L1$ and $L2$ Lagrangian points, disk material enters the Roche lobe in the form of two gas streams. Shocks occur within the Roche lobe as the gas streams collide, and shocks lead to rapid inflow toward the planet within much of planet's Roche lobe. Shocks also propagate in the inner and outer disks that orbit the star. For higher mass planets (of order 6 M_J), the flow rate onto the planet is considerably reduced, which suggests an upper mass limit to planets in the range of 10 M_J. This rate reduction is related to the fact that the gap width increases relative to the Roche (Hill sphere) radius with increasing planetary mass. The flow in the gap affects planetary migration. For the 1 M_J planet case, mass can penetrate from the outer disk to the inner disk, so that the inner disk is not depleted. The results suggest that most of the mass in gas giant planets is acquired by flows through gaps.

Subject headings: accretion, accretion disks — hydrodynamics — methods: numerical — planetary systems — solar system: formation

1. INTRODUCTION

A gas giant planet is believed to form by the accretion of gas from a protoplanetary disk onto a solid core (see review by Lissauer 1993). For typical parameters appropriate to protoplanetary disks, a planet of mass 1 M_J is expected to open a gap about the orbit of the planet (Lin & Papaloizou 1986, 1993). This result comes about because the tidal torques exerted on the disk by the planet (which act to open a gap) are able to overcome the viscous torques (which act to close the gap) (Goldreich & Tremaine 1978). This balance of torques suggests that for planet masses greater than about 1 M_J, a gap is cleared in the disk. In this picture, the formation of the gap terminates the planet's growth.

Simulations of smoothed particle hydrodynamics (SPH) indicate that for eccentric binary star systems, the torque balance argument correctly predicts the gap locations (Artymowicz & Lubow 1994). However, disk material that surrounds a binary system is sometimes able to penetrate the gap and accrete onto the binary (Artymowicz & Lubow 1996, hereafter AL96). The flow is highly nonaxisymmetric and takes the form of two gas streams that are initiated at two corotational points (analogous to Lagrangian points) of the eccentric potential. Under some circumstances, this flow could be quite efficient. That is, the accretion rate through the gap could be comparable to the rate that occurs if the binary were replaced by a single star, so that there is no tidal field to interfere with the flow. AL96 specu-

lated that a similar process could occur in the case of flow onto planets. Continued accretion in the presence of a gap may be of importance in understanding the formation of the recently discovered high-mass (several Jupiter masses) extrasolar planets (e.g., Mayor, Udry, & Queloz 1998; Marcy & Butler 1998).

In this paper, we describe results from numerical simulations of the interactions of planets with protostellar disks. The planet is assumed to be in a circular orbit about the central star. The planet's orbital radius is fixed in these simulations, and effects of planetary migration (e.g., Lin, Bodenheimer, & Richardson 1996; Ward 1997) are ignored. Some early work was carried out by Miki (1982). This study recognized many of the global aspects of the flow but did not address the issue of accretion onto the planet. Studies similar to the one described here have been recently reported upon by Bryden et al. (1999) and Kley (1999). The results presented here provide the highest resolution to date. We are able to determine properties of the flow within the planet's Roche lobe.

The outline of the paper is as follows. Section 2 describes the computational procedure while § 3 describes some tests of the simulation code. Section 4 provides results for a 1 M_J planet, and § 5 provides some results for higher mass planets. Section 6 discusses migration. Section 7 contains a comparison with other studies, and § 8 has the summary and discussion.

2. COMPUTATIONAL PROCEDURE

2.1. *Basic Equations*

Protostellar disks are fairly thin (e.g., Burrows et al. 1996). A typical protostellar disk is expected to have a thickness to radius ratio $H/r \simeq 0.05$–0.1. Because of this, the

[1] Space Telescope Science Institute, 3700 San Martin Drive, Baltimore, MD 21218; lubow@stsci.edu seibert@stsci.edu.

[2] Johns Hopkins University, Department of Physics and Astronomy, 34th and Charles Streets, Baltimore, MD 21218.

[3] Stockholm Observatory, S-133 36 Saltsjobaden, Sweden; pawel@astro.su.se.

disk is approximated as two-dimensional by vertically averaging the three-dimensional fluid equations over height. Although the vertical averaging retains much of the main character of the flow, in some regions of space the approximation is marginally satisfied. In particular, near the Roche lobe of the planet, the disk thickness is not very small compared with the radial length scale of the flow (the ratio is about 0.3).

We assume a viscous model for the disk turbulence, with the usual α disk prescription. The viscous forces are represented by a Navier-Stokes viscosity force per unit area, f. The flow is analyzed in the orbital frame that rotates with the angular speed of the planet Ω_p. In this frame, the flow achieves a near steady state. We adopt cylindrical coordinates (r, θ) with associated flow velocities in the rotating frame $\boldsymbol{u} = (u_r, u_\theta)$. The origin of the coordinate system is taken to be the center of the star. (We ignore the slight center-of-mass shift caused by the planet.) The disk self-gravity is ignored. The equations of motion for the disk of surface density Σ are

$$\frac{\partial \Sigma}{\partial t} + \nabla(\Sigma \boldsymbol{u}) = 0 , \tag{1}$$

$$\frac{\partial p_r}{\partial t} + \nabla(p_r \boldsymbol{u}) = \Sigma r(u_\theta/r + \Omega_p)^2 - \frac{\partial p}{\partial r} - \Sigma \frac{\partial \Phi}{\partial r} + f_r , \tag{2}$$

and

$$\frac{\partial j}{\partial t} + \nabla(j \boldsymbol{u}) = -\frac{\partial p}{\partial \theta} - \Sigma \frac{\partial \Phi}{\partial \theta} + r f_\theta , \tag{3}$$

where $p_r = \Sigma u_r$ is the radial momentum per unit area, p is the vertically integrated gas pressure, $j = \Sigma r(u_\theta + \Omega_p r)$ is the gas angular momentum per unit area, Φ is the gravitational potential in the orbit plane caused by the central star and the planet, and (f_r, f_θ) is the viscous force per unit area that describes the effects of disk turbulence. The gravitational potential Φ is smoothed in the neighborhood of the planet with

$$\Phi(r) = -\frac{GM_s}{r} - \frac{GM_p}{[|\boldsymbol{r} - \boldsymbol{r}_p|^2 + r_{sm}^2]^{1/2}} , \tag{4}$$

where M_s and M_p are the star and planet masses respectively, $\boldsymbol{r}_p$ is the planet location and r_{sm} is the smoothing length of the planet's potential. Typically, we have chosen the smoothing length to be 0.2 times the size of the planet's Roche lobe or $r_{sm} = 0.2a[M_p/(3M_s)]^{1/3}$, where a is the radius of the orbit. The smoothing length did not play an important role in our calculations. We have run models with a smoothing length of zero and found no important differences in the general flow properties.

Equations (1), (2), and (3) express conservation of mass, the radial momentum, and the angular momentum equations, respectively. Equation (3) is written in terms of the angular momentum j, rather than the azimuthal momentum p_θ in the rotating frame. The reason is that the j equation provides better numerical stability (Kley 1998).

The equation of state is taken to be locally isothermal, $p \propto \Sigma T$, with the temperature expressed as a specified function of radius, $T(r)$. This equation of state is appropriate for a gas that radiates internal energy gained by shocks with high efficiency. The viscosity force f is assumed to be the standard Navier-Stokes force (see eq. [15.3] of Landau & Lifshitz 1975). The coefficient of shear viscosity μ represents the effects of disk turbulence, while the bulk viscosity coefficient ζ is set to zero. The value for the kinematic turbulent viscosity $\nu = \mu/\Sigma$ is expressed in terms of the usual α prescription of Shakura and Sunyaev (1973). Namely, for a disk with local sound speed c_s and thickness H, dimensionless parameter α is defined through

$$\nu = \alpha c_s H . \tag{5}$$

The use of the α prescription for disks imposes some simplifications. The actual disk turbulence may well be magnetic in origin (Balbus and Hawley 1991). The full effects of MHD turbulence and the associated nonturbulent magnetic field effects are likely more complex. The interaction of waves in the disk with the turbulence involves additional complexities because the wave-forcing timescale can be shorter than the turnover timescale for the largest eddies. However, the main purpose of the disk viscosity is to provide a mass accretion toward the vicinity of the planet. The details of the turbulence might not be critical for understanding the flow properties near the planet, where tidal forces from the planet are strong.

Equations (1), (2), and (3) are integrated at each time step to provide new values for Σ, p_r, and j, which in turn determine the new values of u_r and u_θ. The above equations are nondimensionalized so that the unit of time is the inverse of the planetary orbital frequency Ω_p. The unit of distance is the orbital radius of the planet a. The unit of gas density in the disk is M_d/a^2, for a disk of (simulated) mass M_d.

2.2. Numerical Method

We have based our calculation on the ZEUS3D code in two dimensions (Stone & Norman 1992). The code was modified to include a standard Navier-Stokes viscous force term. The ZEUS code uses operator splitting in which explicit time derivatives on the left-hand sides of equations (2) and (3) are determined by the terms (called source terms) that appear on the right-hand sides of their respective equations. Divergence terms on the left-hand sides of the equations (1)–(3) contribute additional changes in each time step.

The equations are solved on a spatial grid in the r and θ directions. The code allows for variably spaced gridding, which permits us to obtain higher resolution in the neighborhood of the planet. The time steps satisfy the usual Courant condition, for which we have adopted Courant number 0.5. The code provides an artificial viscosity term, but since we introduce a Navier-Stokes viscous force, we suppress this artificial viscosity. Of course, the code has some intrinsic artificial viscosity because of the finite gridding. For a uniformly spaced mesh, the code is formally second-order accurate in space and first-order accurate in time. For variably spaced meshes, the code is formally first-order accurate in space. But, a high level of accuracy and resolution can be attained by limiting the fractional change in mesh spacing between adjacent cells to be small, of order 1%. The van Leer interpolation option was used.

2.3. Boundary Conditions

The code involves the use of a set of two *ghost* zones that reside beyond the inner and outer boundaries. They are needed to provide spatial derivatives for quantities in the active zones (zones in the simulated region of space) near the boundary. The ghost zones were initialized using the same equations as the active zones. In this way, the velocities in the ghost zones of a Keplerian disk retain the

Keplerian shear. The ghost zones get updated at each time step to provide a spatially smooth variation with the active grid zones. The smoothness is important for the viscous force terms, which depend on the second derivatives of velocity components.

Boundary conditions need to be specified at the inner and outer radial boundaries. (The azimuthal boundary conditions require periodicity in θ.) For some boundary conditions, highly unstable behavior was found. If the flow has a steep density profile near the boundary, then a reflecting or outflow boundary condition can be applied. For a reflecting boundary condition, the code sets the radial velocities of the two ghost zones to the sign-reversed values of radial velocities in the second and third sets of active zones from the radial boundary. That is, the radial velocities of the ghost zones are reflected values of the active zones. In addition, the radial velocities in the active zones closest to the radial boundary are set to zero. For an outflow boundary condition, the code sets the radial velocities of the active zones closest to the radial boundary to zero, if the velocity is directed away from the boundary (inflow). Otherwise, the radial velocity is left unchanged (for outflow).

If the density distribution is fairly flat in radius near the boundary, then an inflow-outflow boundary condition can be applied. This boundary condition lets material flow into or out of the active (simulated) region of the system. The inflow-outflow boundary condition does not change the velocities in the active zones near the boundaries. To provide smooth spatial behavior with this boundary condition, we update the ghost zones with a *constant acceleration* scheme. This is done by applying the changes in physical quantities of the ghost zones at each time step by an amount equal to the changes in nearby active zones.

3. TESTS OF THE CODE

We have carried out some tests of the code for accretion disks. They were performed in the inertial frame without a planet, so that Ω_p and M_p were taken to be zero in the dynamical equations (1)–(3). In one case, we checked on the stability of an orbiting disk of initially constant surface density and pressure. The disk sound speed was constant in time and space, such that H/r was set to 0.1 at the radial midpoint of the simulated region, and the viscosity parameter α was set to zero. The disk was taken to have a ratio of outer to inner radii equal to 3. The zoning was 80 by 80, considerably cruder than our planetary simulations. Inflow-outflow boundary conditions were applied at the radial inner and outer boundaries. The disk was stable, with density fluctuations less than 1% for over 100 orbits, as measured at the disk midpoint. Although this test may seem trivial, it did reveal several problems with our early use of the code. For example, with a uniformly spaced grid, dynamical instability was found at the disk inner edge. This instability was suppressed through the introduction of variable mesh spacing or a small level of viscosity in the Navier-Stokes term f, both of which are used in our planetary simulations.

In another test, we set up a narrow axisymmetric ring of gas that surrounds a central-point mass. The evolution of the ring was followed numerically and compared with the analytical solution of a viscous ring (Pringle 1981). Since the rate of spreading depends on the viscosity, the test provides a means of checking the value of the imposed viscosity parameter α in the Navier-Stokes force f_θ. An 80 by 80

uniform grid was used, with a ratio of outer to inner radii equal to 3. The outflow boundary condition was applied at the radial inner and outer boundaries. The density evolution closely followed the analytical solution (to within a few percent) for several values of viscosity $\alpha \geq 10^{-4}$. The evolution was followed over timescales sufficiently long for substantial profile evolution to occur (40–100 orbits at the disk midpoint). With the Navier-Stokes term set to zero, the evolution was very slow. The equivalent level of artificial viscosity intrinsic to the code was $\alpha \ll 10^{-4}$.

4. SIMULATION OF A 1 M_J PLANET

4.1. *Boundary and Initial Conditions*

The planet was assumed to be able to accrete material without substantial expansion of its radius on the scale of its Roche lobe. The planet was fixed on a grid point in the corotating frame at location $r = 1$, $\theta = \pi$. To simulate the accretion of material by the planet, material that surrounds some region about the planet was nearly fully removed from the simulation in each time step. A residual density of 1.75×10^{-5} (in units of M_d/a^2) was retained in these zones, about 0.1% of the main disk density near the gap. The removed material was assumed to be accreted onto the planet, although the mass of the planet was not increased because of the accretion. The four cells that surround the planet were chosen to be the region of evacuation. The evacuation produces a pressure force that is directed toward the planet, although this pressure force is small compared with other dynamical forces.

We imposed reflecting boundary conditions at the disk inner edge and inflow-outflow boundary conditions at the disk outer edge. The disk inner edge was located at $r = 0.3$ (in units of planet orbital radius a), and the disk outer edge was located at $r = 6$. A variable grid of 252 by 320 was applied, with highest resolution close to the planet. The grid was uniform in both r and θ in a region that included the planet's Roche lobe. With this resolution, the Roche lobe of the planet contained approximately 250 cells.

A temperature profile $T(r) \propto r^{-1}$ was used at all times. The temperature was normalized such that $H/r = c_s/(\Omega_p r) = 0.05$ at $r = 1$. The kinematic disk viscosity v was set to 10^{-5} (in dimensionless units of $a^2\Omega_p$), independent of radius or time. This corresponds to a disk viscosity parameter $\alpha = 4 \times 10^{-3}$ at $r = 1$ (see eq. [5]).

The initial disk-density profile was chosen to be axisymmetric and to follow $\Sigma(r) \propto r^{-1/2}$, together with a low constant density "gap" imposed near the planet. The initial gap size and structure were estimated by an approximate torque balance condition between viscous and tidal torques near the planet. The gap density was about 1.75×10^{-4} or about 1% of the disk density just outside the gap. Computer time was saved by imposing the initial gap, because a smaller and less violent disk adjustment was required to reach a steady state. The gap partitions the disk into regions interior and exterior to the planet. These regions will be referred to as the inner and outer circumstellar disks, respectively.

4.2. *Mass Accretion Rate onto the Planet*

Figure 1 plots the azimuthally averaged surface-density profiles at various times for a 1 M_J planet. The profile achieved a steady state by 100 planetary orbits. The profile indicates the presence of nonlinear waves in the outer disk.
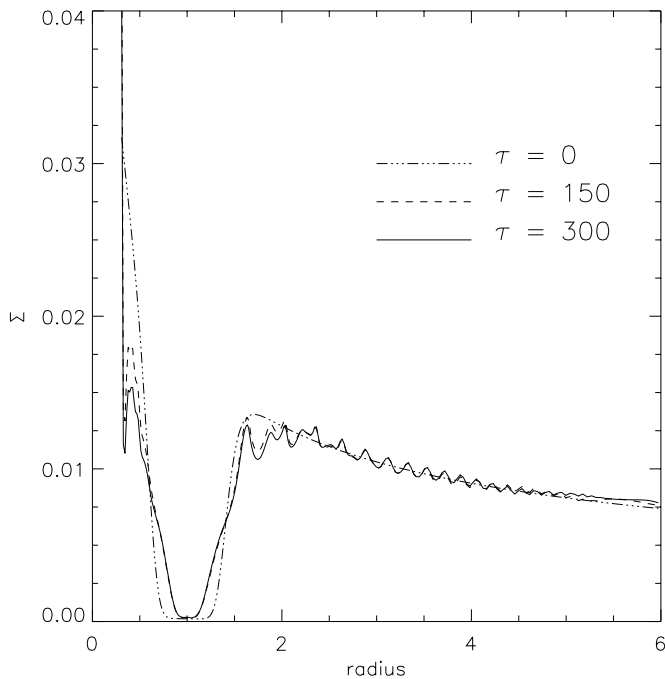
FIG. 1.—Azimuthally averaged surface-density profiles of a disk containing a planet at various times. Density is normalized by M_d/a^2, where M_d is the simulated disk mass and a is the planetary orbital radius. The horizontal axis is normalized by a. A 1 M_J planet resides at $r = 1$, and a 1 $M_\odot$ star is located at $r = 0$. The disk properties are described in § 4.1. The dash-dotted line is the initial density profile, the dashed line is the profile at 150 planetary orbits, and the solid line is the profile at 300 planetary orbits.

The outer disk was well resolved and the density variations near the outer boundary were rather smooth. The inner disk was not resolved as well, and there is discontinuous behavior of the density at the innermost zones. This is partly because of its more rapidly varying density and velocity with radius. The inner boundary flow limited the time steps of the code.

As seen in Figure 2, the planet opens a gap in the disk and causes waves to propagate in the inner and outer circumstellar disks. In the outer disk, the waves damp considerably before reaching the outer boundary. As seen in Figure 3, the mass accretion rate onto the planet becomes fairly steady after about 150 orbits. The accretion rate corresponds to a gain in planetary mass of 2.7×10^{-5} M_d per planetary orbit. For a typical disk mass of 0.02 $M_\odot$, this corresponds to a mass accretion rate of 5.4×10^{-4} M_J per orbit or a mass-doubling timescale of about 2×10^4 yr at the orbit of Jupiter. Since this timescale is much shorter than the disk lifetimes, estimated as a few million years (Walter et al. 1988; Strom, Edwards, & Strom 1989; Beckwith & Sargent 1993), this accretion flow in the presence of a gap can substantially add mass to the planet.

The accretion rate onto the planet can be compared with the rate that would occur if the planet were not interfering with the accretion flow. The accretion efficiency $\mathscr{E}$ is then defined by

$$\mathscr{E} = \frac{\dot{M}}{3\pi\nu\Sigma} , \qquad (6)$$

where Σ is a characteristic density value just outside the gap. In the absence of a planet, the efficiency $\mathscr{E}$ is unity. For the present case, $\mathscr{E} \simeq 2$, which suggests that the flow is quite

efficient. Efficiencies greater than unity are possible because of the gradients imposed by the gap.

4.3. Flow Regions

Figure 4 provides a closer view of the region near the planet in Cartesian coordinates after 250 simulated planetary orbits. The star is located to the right of the figure at $x = 0$, $y = 0$. The left (right) plus sign denotes the outer (inner) Lagrangian point L2 (L1). The Roche lobe containing the L1 point is plotted. The density image shows spiral arms caused by shocks. These shocks within the Roche lobe are separate from those seen in Figure 2 within the circumstellar disk. The shocks within the Roche lobe are clearly seen as discontinuities in the velocity map of Figure 5.

The streamlines are shown as the dashed lines in Figure 4. Critical streamlines that separate the distinct flow regions are shown in solid white lines. The critical streamlines are labeled and sometimes overlap. For example, streamlines labeled a and b in the lower left-hand portion of Figure 4 overlap with each other but then bifurcate at the X-point located near the L2 point. Material in Figure 4 to the left of critical streamline a is outer disk material within the gap (the gap is also seen in Fig. 2). Material between streamlines b and c forms a gas stream that accretes onto the planet. Material below streamline d is on nonaccreting horseshoe orbits. Analogous statements can be made about the other streamlines, which surround the L1 region. Over an entire orbit about the star, the streamlines do not close. So streamlines close to a critical streamline leaving Figure 4 sometimes return as a streamline on the opposite side of the critical streamline, as will be discussed later.

4.3.1. Circumstellar Disks

Gap material associated with the inner and outer disks is *locally* deflected away from the planet by shocks (to the left of streamline a and the right of streamline h). The local shock deflection of material in the inner and outer disks is in the direction away from the planet. Such a deflection is expected on the basis of the theory of spiral shocks (see, e.g., Roberts & Shu 1972 in the context of galactic shocks). However, this is not the dominant effect over an entire orbit. Viscous forces act between shocks to drive material in the outer disk toward the planet. This finding is not surprising, because the outer disk is behaving like an accretion disk that feeds material to the planet. Viscous forces are also responsible for driving material from the inner disk outward toward the planet. Part of this effect is caused by the reflecting inner boundary condition.

4.3.2. Accretion Streams

The material between streamlines b and c and between f and g forms narrow gas streams that penetrate the Roche lobe and ultimately become accreted by the planet. Figure 6 shows the mass flux across dotted line AD in Figure 4. The mass flux monotonically decreases from the disk to the gap regions (from point A to point D). The stream mass flux is peaked near outer bounding streamline b and diminishes toward inner streamline c.

As seen in Figures 4 and 5, the material between streamlines b and c undergoes a shock as it approaches the Roche lobe. This shock is part of the global spiral shock wave visible in Figure 2. As a result, material in the L2 region has a very low velocity in the corotating frame of the planet. In fact, at the X-point the velocity is zero. The material
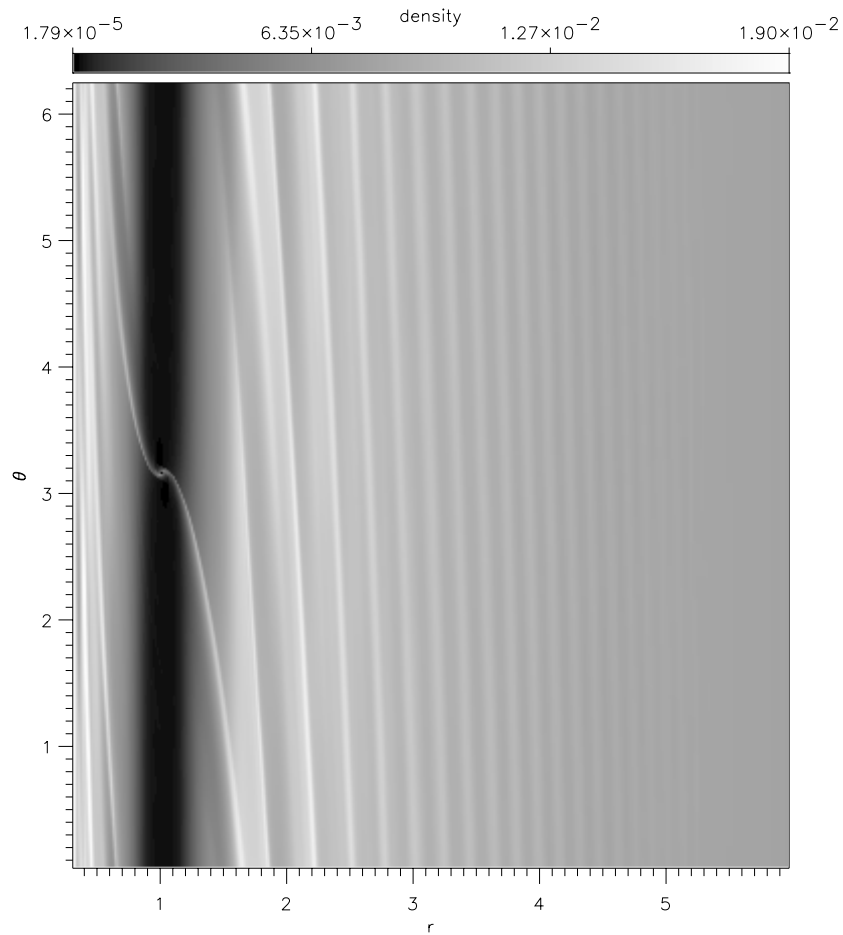
FIG. 2.—Density image of the disk after 300 planetary orbits. The vertical direction is the angle θ about the star. The horizontal direction is the radius r from the center of the star. The planet is located at $r = 1, \theta = \pi$.
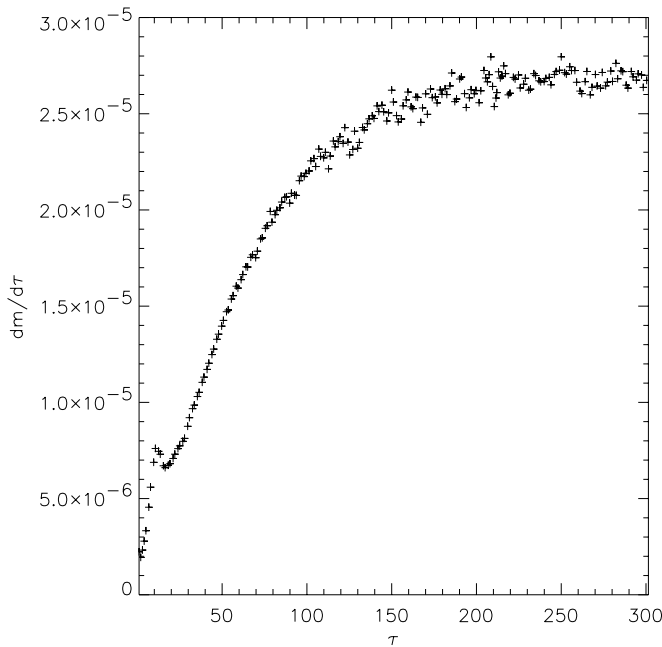

FIG. 3.—Mass accretion rate onto a 1 M_J planet versus time. The accretion rate is expressed in units of the disk mass M_d per planetary orbit, and the time is in units of planetary periods. Each point represents the mass accretion rate averaged over one planetary orbit.

between streamlines b and c then accelerates as it falls into the deeper potential within the Roche lobe and forms the accretion stream. The stream bears some similarity to those in Roche lobe overflow of close binary stars (Lubow & Shu 1975). The resulting counterclockwise flow circulation about the planet is fundamentally determined by Coriolis deflection. The pressure forces play a more important role here than in the binary star case because of the relatively small size of the Roche lobe. (Roche lobe overflow theory predicts that the region of space where pressure, gravitational, and inertial forces are comparable is of order c/Ω_p in size. For giant planets, this region is comparable to the radius of the Roche lobe.) In addition, the presence of two gas streams causes additional interactions communicated by pressure.

The streams undergo a strong shock on the opposite side of the Roche lobe (180° away) from their entrance because of their mutual collision (see Figs. 4 and 5). Following this shock, the streams lose a considerable amount of their angular momentum about the planet and execute highly eccentric orbits. The material spirals inward toward the planet as a result of successive shocks. The shock waves about the planet show signs of weakening close to the planet. The flow region close to the planet (~ 0.2 of the Roche lobe size) shows some indication of a more circular Keplerian flow pattern, although the resolution in this
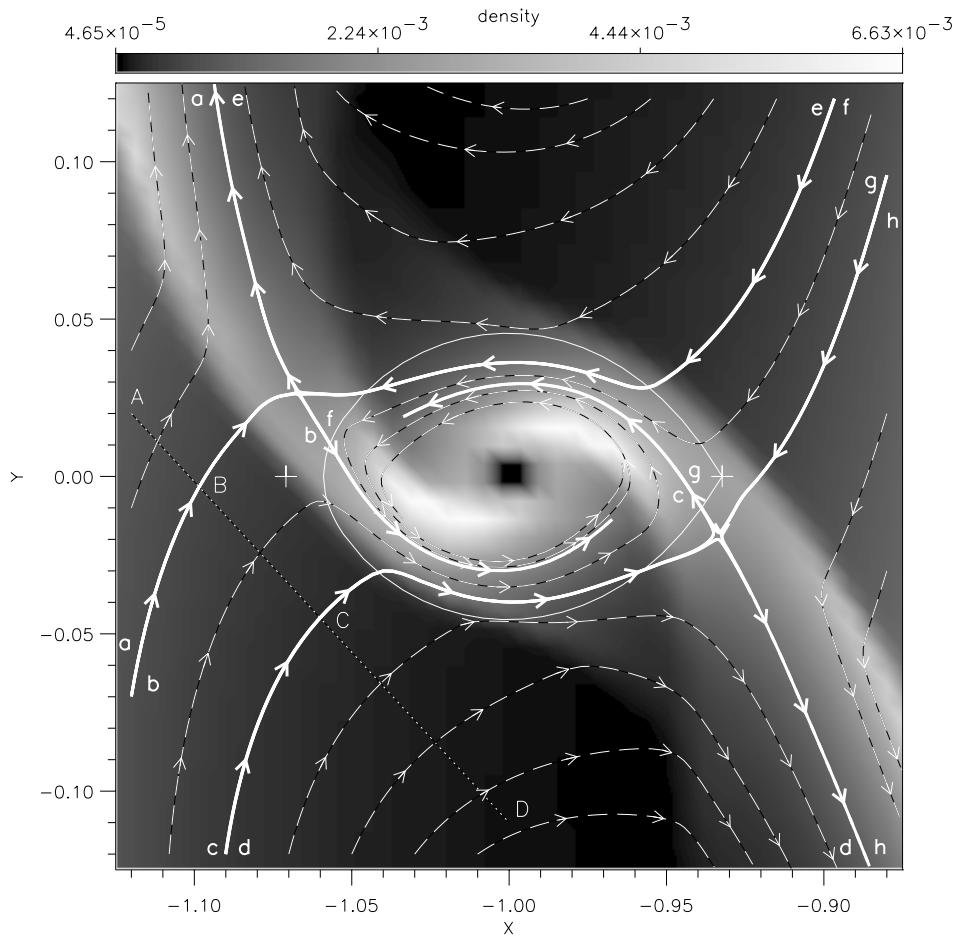
FIG. 4.—A high-resolution density image (in Cartesian coordinates) of the Roche lobe region about a 1 M_J planet. The planet is at location $x = -1$, $y = 0$, and the star is located at the origin. The left (right) plus sign marks the $L2$ ($L1$) point. Sample streamlines are dashed flow lines. Critical streamlines that separate distinct flow regions are solid flow lines (see § 4.3). The dotted line segment AD is used for Fig. 6.
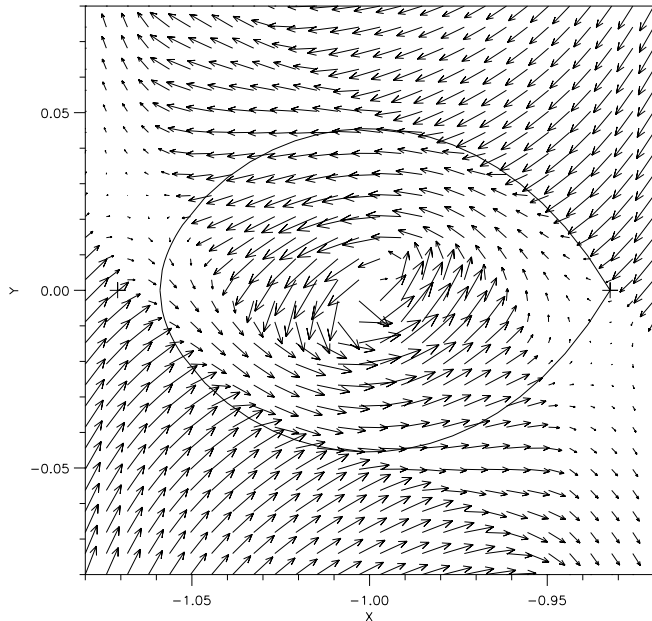

FIG. 5.—A high-resolution velocity map in the corotating frame of the planet (in Cartesian coordinates) of the Roche lobe region about a 1 M_J planet. The planet is at location $x = -1$, $y = 0$, and the star is located at the origin. The left (right) plus sign marks the $L2$ ($L1$) Lagrangian point (see § 4.3).

region is limited. From this inner region, the material is subsequently accreted by the planet.

On the basis of the theory of spiral shocks (Roberts & Shu 1972), the magnitude of radial flow speed u_{rp}, relative to the planet, induced by the shocks about the planet is approximately given by

$$u_{rp} \sim \frac{u_\perp^2}{2\pi u}, \qquad (7)$$

where $u_\perp$ is the flow velocity perpendicular to the shock wave front. As can be seen from Figure 4, velocity $u_\perp \sim u$. The above equation indicates that $u_{rp} \sim u/(2\pi)$. In other words, the shock geometry indicates that the shocks are quite strong and this leads to a fairly rapid radial inflow. The above equation also indicates why the effects of the shocks on the inner and outer disk flows are considerably weaker. Namely, the waves are much more tightly wrapped (see Fig. 2), so that $u_\perp \ll u$ and, therefore, $|u_r| \ll u$.

4.3.3. Horseshoe Orbits

Also seen in Figure 4, the flow well within the gap, but outside the Roche lobe, follows horseshoe orbits (e.g., Dermott and Murray 1981). This region is below streamline d and above streamline e in Figure 4. The horseshoe orbits possess a higher value of Jacobi constant (effective energy) than the inner and outer disk material. The effect of dissi-
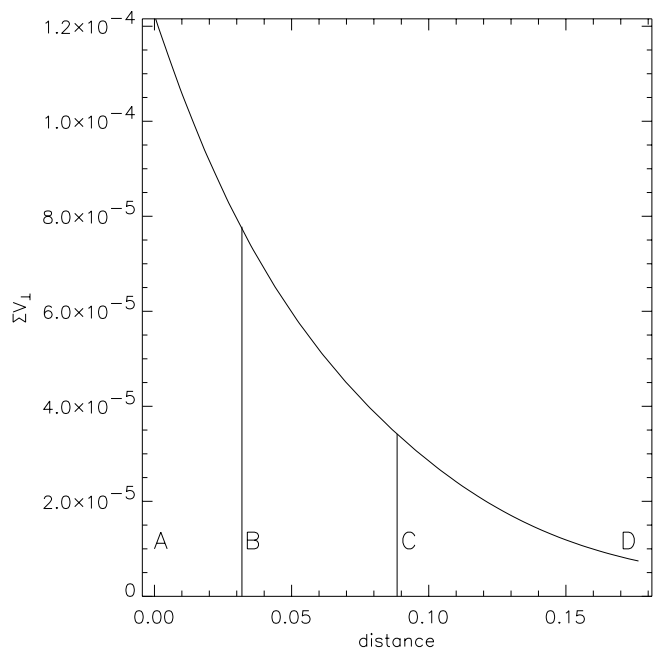
FIG. 6.—Mass flux across dotted line AD in Fig. 4 as a function of distance along the line in units of $M_d \Omega_p/a$ within the disk gap. Position A is in the outer disk region, position B is on the streamline that becomes the outer boundary of the $L2$ accretion stream, position C is on the streamline that becomes the inner boundary of the $L2$ accretion stream, and position D is in the horseshoe orbit region.

pation on horseshoe orbits is to drive material away from the orbit of the planet (out of the horseshoe orbit region).

Figure 7 shows two horseshoe orbits traced by streamlines at a time of 250 planetary orbits. Both horseshoe orbits originate and terminate near $x = 0$, below $y = -1$. As can be seen from Figure 7, the orbits are slightly not closed because of a small outward drift.

4.4. Source of Accretion Streams

The stream material originates from the disk edges in the gap rather than as material on horseshoe orbits. Figure 8 shows some streamlines for material that flows onto the planet. Material within the bounding streamlines that surrounds the left arrow in the figure orbits about the star, and it returns to constitute the $L2$ gas stream that is indicated by the two right arrows in the figure. As seen in the figure, the contribution to the gas stream comes from the disk material in the gap rather than from material in the horseshoe orbit region. At various times, we find fluctuations about this state. Sometimes a small fraction of the stream material does originate from the outermost parts of the horseshoe orbit region, near streamline e in Figure 4. But this material is found, in turn, to originate dominantly from the $L1$ disk region (to the right of streamline h) and so is associated with the horseshoe orbit region only marginally and temporarily. Some slight contribution can come from the decaying horseshoe orbits as seen in Figure 7 (as suggested by Bryden et al. 1999 and Kley 1999). As can be seen
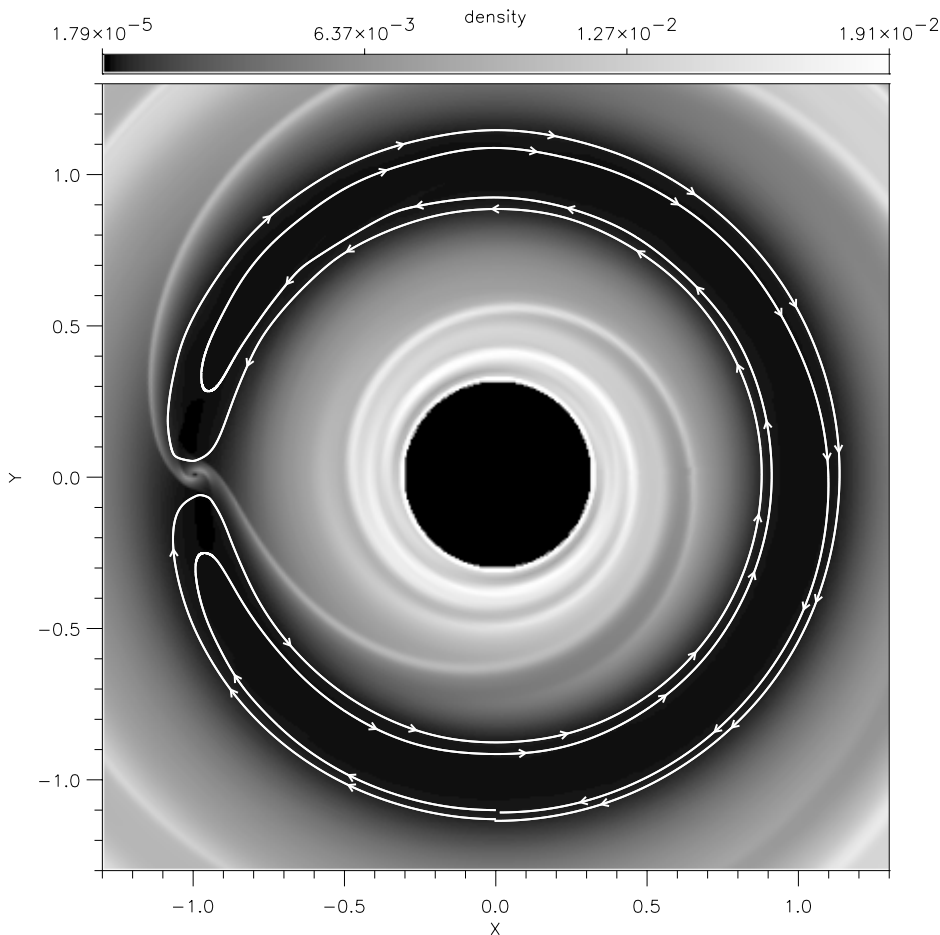

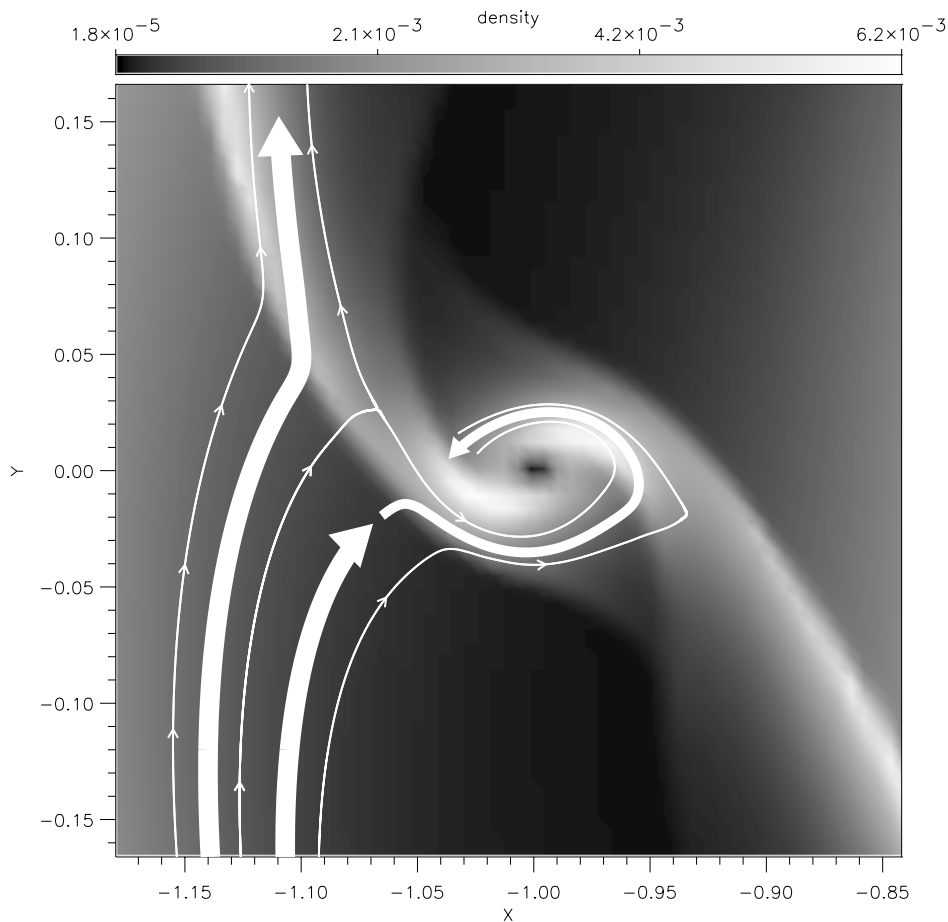FIG. 7.—Two horseshoe orbits within the disk gap (see § 4.3.3)

FIG. 8.—Flow evolution of gas stream material. Material flowing along the left arrow orbits about the star, returns as material that flows along the two right arrows, and becomes accreted by the planet (see § 4.4).

in Figures 4, 5, and 7, the material well within the horseshoe orbit region (below streamline *d* or above streamline *e*) that approaches the Roche lobe is deflected away from the Roche lobe by shocks.

4.5. *Low-Mass Inner Disk*

The reflecting inner-boundary condition applied thus far did not allow material to accrete onto the central star. Consequently, an inner disk was always present in the simulations. The case of an initially low-mass inner disk demonstrates effects at the opposite extreme. We constructed a simulation with the same initial conditions as before, except that densities in the inner disk were set to the density value at the gap midpoint of 1.75×10^{-4}.

A mass buildup of the inner disk occurred at a rate of approximately 5×10^{-5} M_d per planetary period over the 300 simulated orbits. This accretion rate is approximately twice that onto the planet in § 4.2. The efficiency of this flow is $\mathcal{E} \simeq 4$ (see eq. [6]). This effect will likely be reduced when the planet's radial migration is taken into account. This result suggests that the inner disk material within the orbit of a 1 M_J planet will not be depleted to low density by starvation of material from the outer disk.

Figure 9 shows the flow on the scale of the Roche lobe after 150 simulated planetary orbits. In comparison with Figure 4, we see that the $L2$ accretion stream occupies a geometrically smaller region. It also consists of material from the outer disk, with no significant contribution from

horseshoe orbiting gap material. Some material from the outer disk sweeps through the Roche lobe and flows into the newly formed inner disk. Some material from the inner disk has begun to form a weak $L1$ stream of material that flows back onto the planet.

Figure 10 traces a streamline that flows from the outer to inner disks. This streamline begins in the outer disk and circulates about the star in the outer portions of the horseshoe orbit region. It subsequently joins the inner disk flow.

4.6. *Cause of Shocks within the Roche Lobe*

Figure 4 shows that the shock waves in the inner and outer circumstellar disks are quite separate (in azimuthal phase) from the shock waves within the Roche lobe. There are two likely causes of the shocks within the Roche lobe. One possible cause is the resonant generation of a spiral wave by the $m = 2$ component of the tidal forcing provided by the star (see, e.g., Savonije, Papaloizou, & Lin 1994 for the case of a binary star system). The other possibility is a direct impact of gap material being fed into the Roche lobe with material circulating within the Roche lobe. We can use Figure 9 to help discriminate between the two possible causes. If the dominant cause of the shocks is resonant forcing, then the two arms would have equal strength in Figure 9. (We have verified this would be true with this code by simulating a circumplanetary disk without circumstellar disks present.) On the other hand, arms of unequal strength would result in Figure 9, if the shocks in Figure 4 were
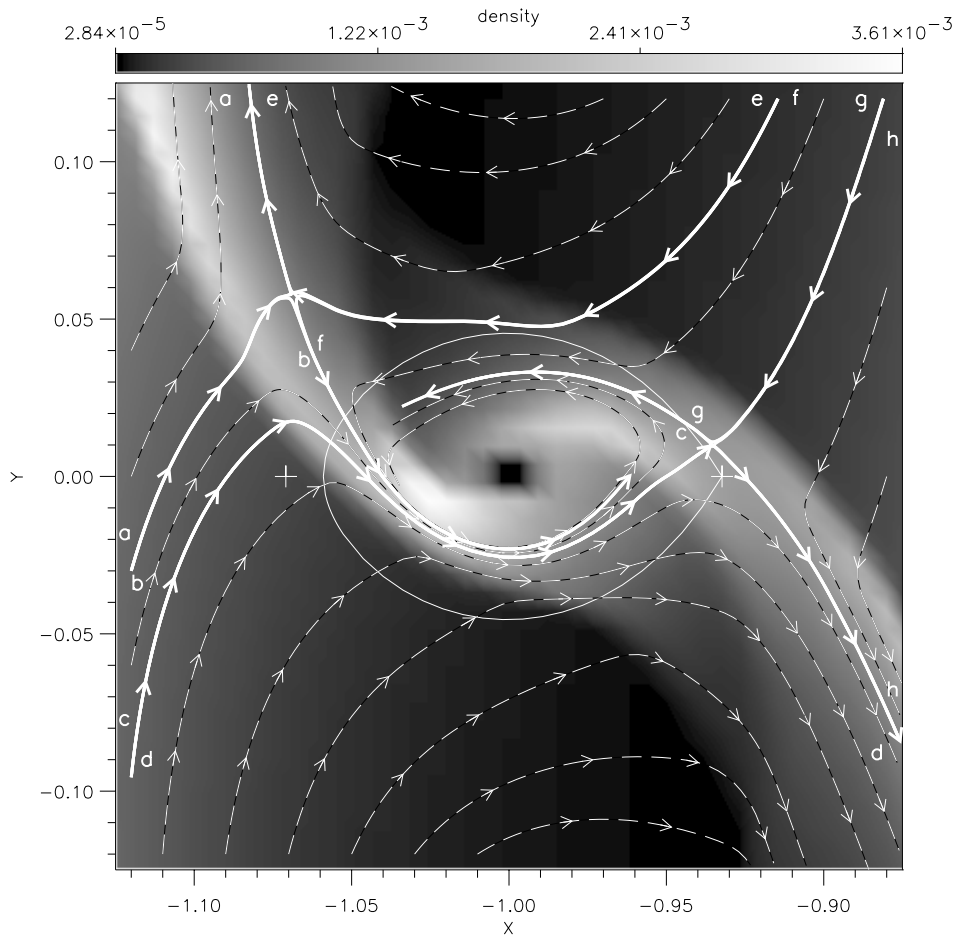
FIG. 9.—High-resolution image of the vicinity of the Roche lobe. Same as Fig. 4, except that the simulation was initialized to have a very small mass inner circumstellar disk (see § 4.5).

formed by the colliding streams. In that case, a one-sided shock structure would be expected in Figure 9 as the stream impacts with itself on the $L2$ side of the Roche lobe. The results in Figure 9 do show a two-arm pattern but with rather different amplitudes in the arms. This suggests that collisions dominate the shock production. Furthermore, it is evident from Figures 4 and 5 that the shocks in the outer region of the Roche lobe are caused by a direct impact from stream material.

5. PLANETS OF HIGHER MASS

We have conducted a series of simulations of the planet accretion from disks with planet masses from 1 to 6 M_J. For historical reasons, the disk conditions were somewhat different from those described in the last section. The disk thickness to radius ratio was taken to be constant in radius with $H/r = c_s/(\Omega_p r) = 0.05$ throughout. The kinematic disk viscosity was chosen to be $v = 10^{-5}$ at $r = 1$, corresponding to an $\alpha = 4 \times 10^{-3}$ at $r = 1$. The model parameters were the same as in the last section at $r = 1$; only their variation in r is different. A uniform r-θ grid of 100 by 300 was used. The Roche lobe flow was not well resolved. The mass accretion rate was determined by evacuating the entire Roche lobe in each time step. Consequently, the absolute values of the accretion rates are not as well determined as in the last section. However, the relative accretion rates for different planetary masses are likely to be better determined than the absolute rates.

Figure 11 shows the accretion rate as a function of planet mass. There is a clear trend for the mass accretion rate to drop with increasing planet mass. This decline is related to the fact that the gap width increases relative to the Roche (Hill sphere) radius with increasing planetary mass. For a planet of 6 M_J, the accretion rate has dropped substantially. The mass accretion rate is smaller by about a factor of 10. Therefore, the timescale to accrete 1 M_J from a 0.02 $M_\odot$ disk increases to several hundred thousand years. For an even higher mass planet, the flow rate would be less. So it would appear difficult, but not impossible, to reach say 10 M_J over the disk lifetime (several million years) under these conditions.

6. MIGRATION

The planets modeled in this paper are subject to radial migration because of their interactions with the gas. The migration occurs in the presence of a gap in the disk (Lin & Papaloizou 1986) and is sometimes called type II migration (Ward 1997). In the case wherein the planet mass is small compared with the disk mass, the planet transmits the disk accretion torque across the gap and is otherwise carried inward along with the accretion flow. The main limitation of the current study in determining the effects of migration is that the planet was not allowed to move radially over the course of the simulation. For a mobile planet, the torque imposed by the disk would adjust to provide migration on the viscous evolution timescale of the disk.
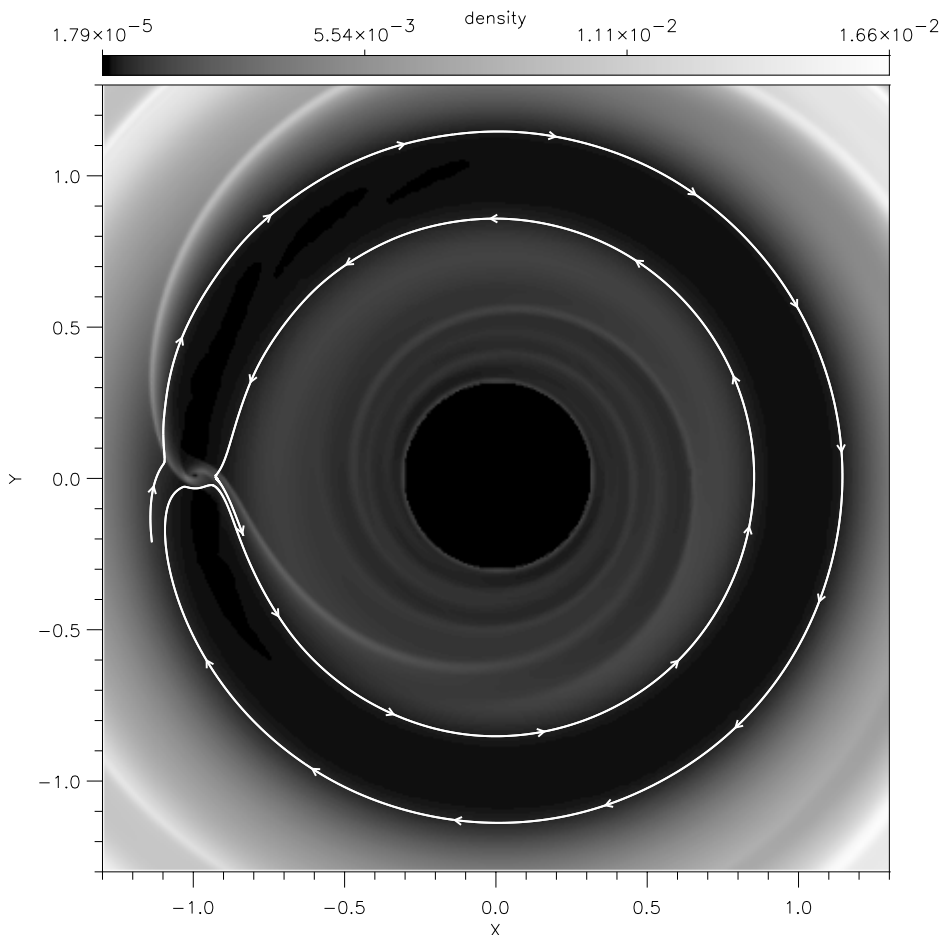
FIG. 10.—Streamline in the case of a depleted inner disk. The streamline starts in the outer disk and enters the inner disk (see § 4.5).
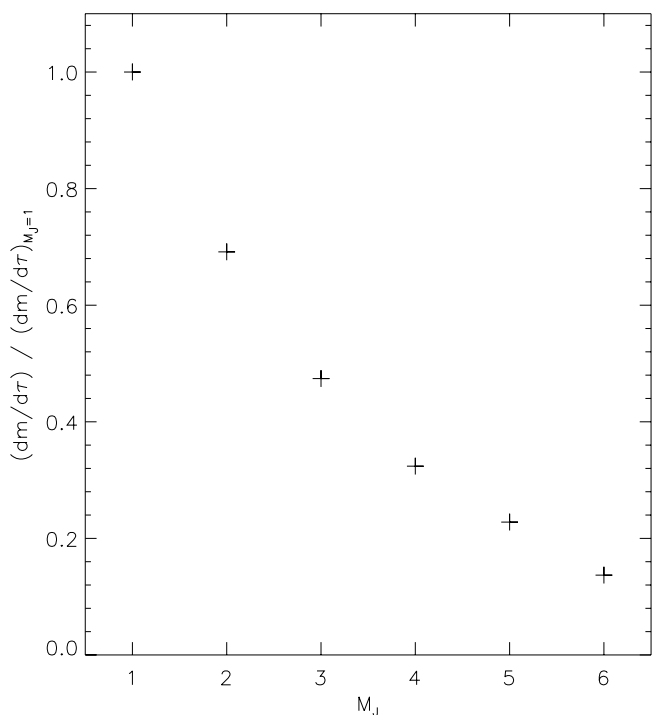

FIG. 11.—Mass accretion rate (normalized by the mass accretion rate onto a 1 M_J planet) as a function of planet mass for planets that orbit a 1 $M_\odot$ star.

There are, however, two limiting cases where the migration effects can be considered based on the results of this paper. In both cases, the application is valid because the migration rate is small. In one case, the planet mass is large compared with the disk mass. Another case occurs when the planet is surrounded by only an outer disk. This situation could arise, for example, if a planet migrates to a central hole in the disk where migration effectively stops, enabling the so-called hot Jupiters to survive capture by the central star (Lin et al. 1996).

Table 1 shows the migration rates caused by the gravitational back reaction of the gas on the 1 M_J planet model of § 4. Contributions to migration come from torques in the four regions of space described in Table 1: the inner disk, inner gap, outer gap, and outer disk. In this terminology, the inner and outer disks refer to the region outside the gap as seen in Figure 2. The inner and outer gap regions contain

TABLE 1

MIGRATION RATE OF A 1 M_J PLANET

Region	Interval	$\dot{a}(2\pi M_s)/(aM_d\Omega_p)$
Inner disk	$0.2a < r < 0.8a$	$+0.0015$
Inner gap	$0.8a < r < 1.0a$	-0.0155
Outer gap	$1.0a < r < 1.2a$	$+0.0135$
Outer disk	$1.2a < r < 7.0a$	-0.0039
Total	$0.2a < r < 7.0a$	-0.0044

all the gas interior and exterior to the planetary orbit, respectively, within the gap. The third column gives the migration rate expressed as $(\dot{a}/a)(2\pi/\Omega_p)(M_s/M_d)$, where a is the orbital radius of the planet and M_s is the mass of the central star. This column expresses the fractional change in the orbital radius per planetary orbit, scaled by the mass ratio of the star to the disk. Torques arise from the non-axisymmetric distribution of material about the planet, as seen in Figures 2 and 4. The individual effects of the inner and outer gaps are strong, about 5 times bigger than the circumstellar disk contributions. However, they nearly cancel by establishing opposing torques on the planet. Their net contribution is an inward migration that is comparable to the net circumstellar (nongap) disk contributions, which cancel less completely between the inner and outer disks. The overall effect is an inward migration at about the same rate as is caused by the outer disk alone. Thus, the situation is not very different from type I migration (Ward 1997).

Consider now the second case, namely, where the planet's migration is halted near the inner edge of the disk. We have computed the resulting migration in such a case. The migration rate corresponds closely to having contributions only from the outer disk and outer gap as indicated in Table 1. The result is that the planet has a net outward migration back into disk because of the gap contribution. On the other hand, if the planet is embedded well within the disk, it will migrate inward, via type II migration. This suggests that the planet may remain in an equilibrium point of no net migration by remaining within the disk and continuing to accrete matter. This equilibrium assumes that gas flows within the gap maintain the torques expected on the basis of these calculations. In reality, these flows may be affected by magnetic fields that are responsible for maintaining the central hole in the disk by carrying material onto the central star (Koenigl 1991; Ostriker & Shu 1995). Therefore, further investigations are needed.

7. COMPARISON WITH OTHER RESULTS

As mentioned in § 1, Bryden et al. (1999) and Kley (1999) have carried out similar calculations but with lower resolution of the Roche lobe region. Our disk conditions were coordinated with those of Kley and show good numerical agreement for the accretion rates. For the same disk mass, the mass accretion rates we obtain are about a factor of 2 less than those of Kley for his model *2q*. The results of the Bryden et al. (1999) study also provide similar accretion rates. Some differences in accretion rates may be because of their lower resolution of the Roche region. The accretion rates are also consistent with preliminary results using the PPM code reported in Artymowicz, Lubow, & Kley (1998).

8. SUMMARY AND DISCUSSION

Our simulations show that a planet of mass 1 M_J or greater opens a gap in a protostellar disk for typical disk parameters (see Fig. 2). However, mass can penetrate the gap and flow onto the planet (see Figs. 3 and 4). For a 1 M_J planet, the flow onto the planet occurs with high efficiency. That is, the accretion rate occurs at about the rate that material would accrete through the planet's orbit in the absence of the planet (and its associated gap). These mass accretion rates are consistent with those found by Bryden et al. (1999) and Kley (1999). This high efficiency was shown by Kley to hold over a wide range of disk turbulent vis-

cosities, even to much smaller values than considered here. This result means that a significant fraction of the next 1 M_J of inflowing disk material exterior to a 1 M_J planet would be accreted by the planet.

The flow near planets follows the main principles that govern the mass flow though gaps around binaries (AL96), although there are some differences. In this picture, mass accretion flows originate at corotation points and take the form of gas streams. In the eccentric binary case, the corotation points were provided by a dominant component of the binary eccentric potential. A large gap encompassed the entire binary and two streams were evident in simulations. The streams represented the highest density material in much of the gap.

In the planetary case, the gap is much narrower because of the relatively small mass of the planet (see Fig. 2). Furthermore, the planet was taken to reside on a circular orbit that limits the number of resonances present. The corresponding corotation points in the circular orbit case are the $L1$ and $L2$ Lagrangian points. As seen in Figures 4 and 5, the flow into the Roche lobe occurs in the form of two gas streams that penetrate at these corotation points. The streams are composed of material that comes from the disk (rather than from the gap horseshoe material), as seen in Figure 8. This disk material undergoes a shock and nearly comes to rest in the corotating frame close to the $L1$ and $L2$ points (see Fig. 5). The material then accelerates toward the planet as gas streams. Each stream undergoes a strong shock at about 180° in azimuth around the planet from the point of penetration because of a collision with the alternate stream (see Figs. 4 and 5).

Subsequent shocks within the Roche lobe drive material fairly rapidly toward the planet. The density peaks within the Roche lobe are dominated by these shocks, which give the appearance of the inner spiral arms in Figure 4. Closer to the planet, there is evidence for a circular Keplerian disk without strong shocks.

For higher mass planets, the mass flow onto the planet weakens considerably (see Fig. 11). This behavior differs from that found for eccentric binary star systems with an assumed higher viscosity, where no apparent tidal limit to the flow was found (AL96). On the other hand, some mass flow does occur through gaps, which apparently can increase planetary masses substantially beyond 1 M_J. The trend seen in Figure 11 is related to the fact that the gap width increases relative to the planetary Roche (Hill sphere) radius with increasing planetary mass. Based on the current calculation, it would appear that tidal truncation might limit planet growth to roughly 10 M_J (see § 5). Such a result would be consistent with the highest mass extrasolar planets. The combined number distribution of planets and spectroscopic binary stars as a function of secondary mass suggests a dip in the range of 7 M_J (Mayor et al. 1998) or 10–30 M_J (Mazeh, Goldberg, & Latham 1998), indicative of a mass upper limit to planets and lower limit to stars in this range.

The circumplanetary disk provides a possible site for the formation of planetary satellites. The sense of rotation of the disk is prograde because of the influence of Coriolis forces on the gas streams. Consequently, the accretion flow provides prograde planetary spins and prograde satellite orbital motion. The more quiescent flow close to the planet (see Fig. 4) may permit a more favorable region for satellite accumulation.

The gas flows can also affect the migration, since they come close to the planet and exert torques (see § 6). Another potentially important effect is planetary eccentricity. The more massive extrasolar planets are observed to be eccentric (see Mazeh, Mayor, & Latham 1996). In some cases, the eccentricity may have been present while the planet was surrounded by a disk, in particular if the eccentricity was generated by planet-disk interactions (e.g., AL96). The mass-flow rate through a gap surrounding an eccentric planet may well be higher than for a corresponding circular orbit planet. An eccentric planet opens a larger gap because of its radial excursions. More resonances occur in such a case and the situation may become closer to that expected for eccentric binary star systems.

REFERENCES

Artymowicz, P., & Lubow, S. H. 1994, ApJ, 421, 651
———. 1996, ApJ, 476, L77 (AL96)
Artymowicz, P., Lubow, S. H., & Kley, W. 1998, in Planetary Systems— The Long View, ed. L. Celnikier et al. (Gif-sur-Yvette: Editions Frontières)
Balbus, S. A., & Hawley, J. F. 1991, ApJ, 376, 214
Beckwith, S. V. W., & Sargent, A. I. 1993, in Protostars and Planets III, ed. E. H. Levy & J. I. Lunine (Tucson: Univ. of Arizona Press), 521
Bryden, G., Chen, X., Lin, D. C. N., Nelson, R. P., & Papaloizou, J. C. B. 1999, ApJ, 514, 344
Burrows, C. J., et al. 1996, ApJ, 473, 437
Dermott, S. F., & Murray, C. D. 1981, Icarus, 48, 1
Goldreich, P., & Tremaine, S. 1978, Icarus, 34, 240
Kley, W. 1998, A&A, 338, L37
———. 1999, MNRAS, 303, 696
Koenigl, A. 1991, ApJ, 370, 39
Landau, L. D., & Lifshitz, E. M. 1975, Fluid Mechanics (New York: Pergamon)
Lin, D. N. C., Bodenheimer, P., & Richardson, D. C. 1996, Nature, 380, 606
Lin, D. N. C., & Papaloizou, J. C. B. 1986, ApJ, 307, 395
———. 1993, in Protostars and Planets III, ed. E. H. Levy & J. I. Lunine (Tucson: Univ. of Arizona Press), 749
Lissauer, J. J. 1993, MNRAS, 31, 129
Lubow, S. H., & Shu, F. H. 1975, ApJ, 198, 383
Marcy, G. W., & Butler, R. P. 1998, ARA&A, 36, 57
Mayor, M., Udry, S., & Queloz, D. 1998, ASP Conf. Ser. 154, Tenth Cambridge Workshop on Cool Stars, Stellar Systems, and the Sun, ed. R. A. Donahue & J. A. Bookbinder (San Francisco: ASP), 77
Mazeh, T., Goldberg, D., & Latham, D. W. 1998, ApJ, 501, L199
Mazeh, T., Mayor, M., & Latham, D. W. 1996, ApJ, 478, 367
Miki, S. 1982, Prog. Theor. Phys., 67, 1053
Ostriker, E. C., & Shu, F. H. 1995, ApJ, 447, 813
Pringle, J. E. 1981, ARA&A, 19, 137
Roberts, W. W., Jr., & Shu, F. H. 1972, Astrophys. Lett., 12, 49
Savonije, G. J., Papaloizou, J. C. B., & Lin, D. N. C. 1994, MNRAS, 268, 13
Shakura, N. I., & Sunyaev, R. A. 1973, A&A, 24, 337
Stone, J., & Norman, M. L. 1992, ApJS, 80, 753
Strom, S. E., Edwards, S., & Strom, K. M. 1989, in Proc. STScI Symp. Ser. 3, The Formation and Evolution of Planetary Systems (Cambridge: Cambridge Univ. Press), 344
Walter, F. M., Brown, A., Mathieu, R. D., Meyers, P. C., & Vrba, F. J. 1988, AJ, 96, 297
Ward, W. R. 1997, ApJ, 482, L211